Chapter 6
Simulation of Process Machine Interaction in NC-Shape Grinding

D. Biermann, H. Blum, A. Rademacher,
A.V. Scheidler, and K. Weinert

Abstract. The study focuses on the NC-shape grinding process when using toroid grinding wheels and its simulation. First, the experimental investigation with respect to the machine structure and its dynamic behavior, the process forces as well as the temperature distribution in the workpiece and the grinding wheel are discussed. That forms the basis for the modeling and simulation of the NC-shape grinding process. The simulation consists of a geometric-kinematical simulation coupled with a finite element simulation. To validate the simulation, comparisons between the quantities measured and the corresponding calculated values are carried out. Subsequently to this validation the transferability of the simulation to other grinding processes is studied. Furthermore, the simulation is utilized to optimize grinding processes, especially with respect to the NC data.

6.1 Introduction

Grinding processes are mainly used as surface finishing processes. The chip removal is usually carried out by rotating grinding wheels with bonded abrasive grains. The process is characterized by high cutting speeds and various contacts between the workpiece and the single grains. Grinding is usually the last step in the production chain of a workpiece and, accordingly, this phase plays a very important role. On account of this, defects caused by the grinding process would be associated with high costs and must be avoided.

A toroid grinding wheel can be flexibly used for NC-shape grinding. Based on the semi-circular profile of the grinding wheel and a line-by-line movement it is possible to machine geometrically-complex surfaces. The different parameters related to NC-shape grinding with a toroid grinding wheel are demonstrated in Fig. 6.1. The feed motion in the NC-shape grinding process is controlled by NC-data, which provides excellent possibilities for grinding free-formed workpiece surfaces. The use of CNC-technology and an adapted path control allows the grinding of planes as well as profiles and complex shapes. The contact area between grinding wheel and workpiece varies during engagement along the tool paths. In the case of complex engagement, the contact area is not measurable without additional software tools. The shape grinding process is determined by the shape of the tool, the kinematic conditions of the cut, the chip removal and the surface produced [1].

B. Denkena and F. Hollmann (Eds.): Process Machine Interactions, LNPE, pp. 121–141.
springerlink.com

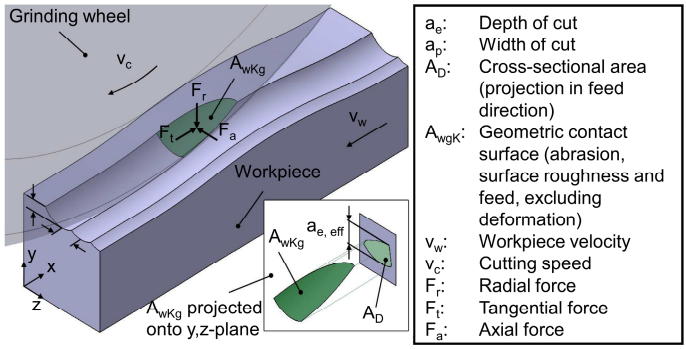

Fig. 6.1 Different parameters of NC-shape grinding with a toroid grinding wheel [2]

The interaction between grinding wheel, workpiece and machine tool in an NC-shape grinding process using a toroid grinding wheel is examined in the present experiments. The research presented in this paper describes the process behavior of the shape grinding process. The description of the interaction between grinding wheel, workpiece and machine tool in a NC-shape grinding process requires various simulation models and corresponding experiments.

In addition to obtaining a basic understanding of the process and its simulation, the application of the simulation and its transferability to other processes are the focus of the current research. Here, application means that the simulation results are used to optimize the NC-shape grinding process. One approach we mainly work on this purpose is the modification of the NC-data in such a way that grinding errors are reduced or eliminated. First results related to path planning are presented in this chapter, where the depth of cut is increased to compensate for the deflection of the grinding machine. It is considerably more difficult to reduce the effect on the workpiece caused by oscillations, which result from the dynamic behavior of the machine, because restrictions relating to the machine tool control of the grinding machine have to be taken into account. With respect to the practical application of the simulation, the transferability of this simulation approach to different grinding machines and other grinding processes is of decisive importance. The simulation is applied to other grinding wheels than the toroid one and the workpiece material varied. Thereby, the parameters in the simulation model are identified and it becomes obvious which parameters have to be adjusted. Furthermore, the dependency of the model's parameters on the modifications is described.

In the next section, we will discuss the experimental basis of the simulation and describe the experiments relating to the dynamic behavior of the machine as well as to measurements of force and temperature. The topic of Section 6.3 is the simulation approach and a detailed description of single constituent parts of the simulation. Furthermore, the determination of the model's parameters using numerical methods is explained. Section 6.4 focuses on the validation of the simulation results. The application of the simulation to path planning and the transferability of the simulation to other grinding processes are examined in Section 6.5. Finally, we will draw some conclusions and provide an outlook on further developments.

6.2 Experimental Results

The accuracy and the dynamic behavior of the structure of the machine were investigated in order to model and simulate the shape-grinding process in its complexity. In shape grinding, material removal occurs along the tool paths, which vary in height. Thus, there is no engagement of the tool in the direction of feed motion. Hereby, in the process, complex and no longer trivially measurable contact surfaces between the tool and the workpiece can occur. In addition, the accuracy of the test machine used must be fundamentally taken into account in order to be able to represent these contact surfaces in a way that corresponds realistically to the process. Static, dynamic and thermal deformations as well as machine induced errors can lead to variances, which cannot be accounted for solely by examining the tool, the contour of the workpiece and the programmed movement in relation to each other. Furthermore, the machine must be suitable for the execution of the programmed target motions. In this section, the measurement of the static and dynamic machine tool behavior and the effects of this behavior on the surfaces of the workpiece, the generated temperatures and the forces are to be discussed.

6.2.1 Measurement of the Static and Dynamic Machine Tool Behavior

The results of the experiments, which were conducted to measure the reactivity of the traversing axes and the static as well as dynamic behavior of the machine structure, will now be presented. First, the positioning accuracy of the machine will be discussed and followed by the description of the dynamic properties of the machine and their effects on the surface of the workpiece.

Examination of the Positioning Accuracy

The positioning accuracy was determined using a laser interferometer. In this way, the absolute positioning error was determined. It appears that the positioning accuracy measured for the z and the y axes for a workpiece width of b_{max} = 20 mm and a maximum profile height of h_{max} = 10 mm lies within the area of tolerance of measurement precision. Slip occurs because of the belt drive of the x axis so that a positioning can be realized only in one direction. Accordingly, the experiments were conducted using down-grinding since small forces occur in this process [2].

The contours of the workpiece resulted from line-by-line traversing movements of the toroid grinding wheel. A large number of grinding strokes with varying amounts of material removal results from the process kinematics until the desired workpiece contour is realized. The process is characterized by a high degree of flexibility. The test machine is designed for a fast workpiece velocity of $v_{w,\,max}$ = 35 m/min in its function as a surface and profile grinding machine. The vertical traversing axis is however limited to traversing speeds of $v_{f,y}$ = 4 m/min. The traversing speed must be constant. When interpolating the x and the y axes the traversing velocity must conform to the slower speed. The interpolation of the machine axes takes place linearly between the sampling points provided by the NC program. Because of this, discontinuous transitions between the path segments result, which lead to a significant faceting of the workpiece surface. Experiments

to determine the maximum traversing speed when the distance between the NC-data points is $\Delta = 0.5$ mm have shown that the machine reaches a maximum workpiece velocity of $v_w = 2238$ mm/min because the drive dynamics of the machine using this NC-data points is limited. This has to be taken into account during the shape grinding processes [2].

Dynamic Behavior of the Machine Structure

During the grinding process, forces are generated by the contact of the grinding wheel with the workpiece, which directly affect workpiece quality or have an effect on the machine parts lying in the distribution of force. The grinding machine system can thereby be induced to vibrate. Such a coupled system is determined by mutual interaction between the machine structure and the process. The dynamic behavior of the system is investigated in order to reach a better understanding of the cause of the waviness and to be able to represent this in a simulation. For this purpose, a modal analysis is conducted. The grinding machine is converted into a simplified substitute model in order to determine the modal parameters. The substitute structure is brought close into line with the grinding machine by using a total of 106 nodes. The substitute system is understood to be dynamically linear, i. e. we proceed on the assumption that a proportionality exists between excitation and response. The linearity of the system is the pre-condition for ascertaining the frequency response function [2].

Several modes arise from the modal analysis of the grinding machine, three of which are largely identical with the frequencies found by measuring the flexibility at the spindle. The related eigenfrequency forms are presented in Fig. 6.2. Basically, no significant relative displacements between the workpiece and the tool could be seen at eigenmodes having a frequency of $f < 50$ Hz so that an influence on the process and thus on the quality of the workpiece can be excluded here [2].

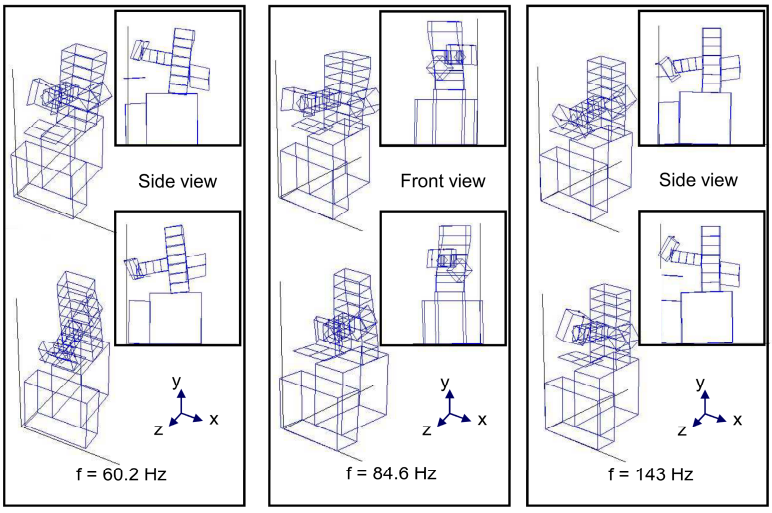

Fig. 6.2 Eigenmodes of the grinding machine investigated as determined by the modal analysis along with a representation of the extreme position of deflection [2]

Two eigenmodes play an important role when dynamic forces in a vertical direction affect the machine. Engaging the grinding wheel with the workpiece causes a waviness with an eigenfrequency of $f = 60.2$ Hz. A strong vertical oscillation of the spindle tower can be seen at this frequency, so the grinding spindle with its tower oscillates along the y axis. The second eigenmode has an effect in the vertical direction at an eigenfrequency of $f = 143$ Hz and represents its effect through a vertical oscillation of the spindle. The spindle executes a horizontal oscillating movement parallel to the machine table at an eigenfrequency of $f = 84.6$ Hz [2].

6.2.2 *Force Measurement*

The process forces are to be determined in order to develop a force model in the simulation. These forces increase with increasing depth of cut a_e and increasing workpiece velocity v_w. An example of the mean values of the radial forces for various workpiece velocities v_w and depths of cut a_e are shown in Fig. 6.3 [2].

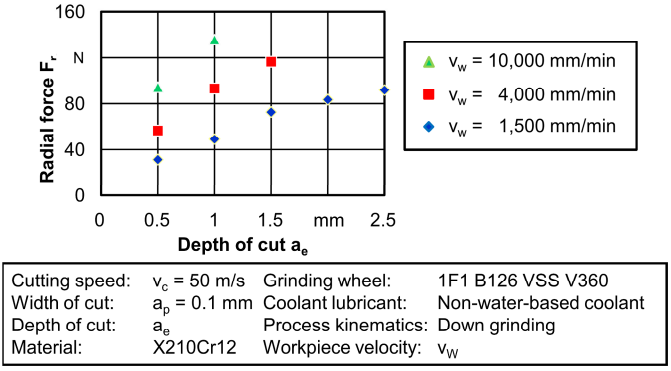

Fig. 6.3 Forces at various depths of cut a_e and workpiece velocities v_w

Determining the Friction in the System

The friction coefficient is calculated by using Coulomb's Law to describe friction. This law is simply an estimation because only a global force during the grinding process can be measured. The friction coefficient calculated is nearly constant for a grinding path in the quasi-stationary area. This coefficient, of course, behaves differently depending on the engagement conditions during run-in and run-out. This is presented for two conditions of engagement in Fig. 6.4. The coefficient of friction also changes when the workpiece velocity v_w and the depth of cut are varied.

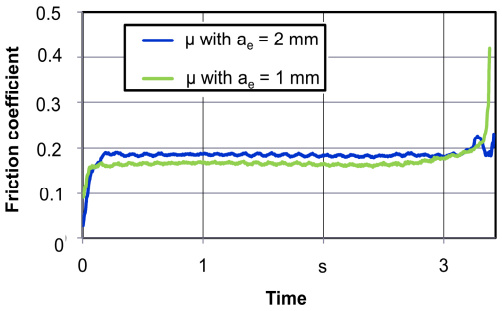

Cutting speed:	v_c = 50 m/s	Grinding wheel:	1F1 B126 VSS V360
Width of cut:	a_p = 0.1 mm	Coolant lubricant:	Non-water-based coolant
Depth of cut:	a_e	Process kinematics:	Down grinding
Material:	X210Cr12	Workpiece velocity:	v_W = 1500 mm/min

Fig. 6.4 Friction coefficients determined for different process parameters along the grinding path

6.2.3 Temperature Measurement

Sect. 1.3.3 showed that temperatures have a considerable effect on the quality of the workpiece. An important influence on temperature development is the coolant supply to the contact area, which is optimized, as described in [3], for NC-shape grinding using toroid grinding wheels. It has been shown that shoe nozzles are best suited for this process because under constant machining parameters the least workpiece damage in terms of grinding burn and cracks on the surface has been found [3].

The process temperatures were measured using thermocouples and a thermographic camera in order to determine the influence of heat development during NC-shape grinding. When measuring with thermocouples, it was seen in [4-7] that the experimental results here, regarding the dependency of the temperature on the parameters workpiece velocity v_w, depth of cut a_e, and the distance between the thermocouple and the surface Δx, are comparable to the main results in case of the toroid grinding wheel. The temperature increases with increasing workpiece velocity and depth of cut and with the decreasing distance between the thermocouple and the surface. An example is shown in Fig. 6.5 [8].

The temperatures measured using the thermographic camera during face grinding are comparable to those found when using the thermocouple measurement technique. For the same distance to the contact area and equivalent process parameters both methods yield similar temperature values. Thus, the thermographic camera technique can be used when machining other surface contours with complex and varying contact areas. It must be taken into account that only free-form, two-dimensional surfaces can be machined because the camera can measure only temperatures close to the workpiece surface. Since convex surfaces are produced during the course of the experiments we conducted, one can get an idea of temperature development when the contact area between grinding wheel and workpiece

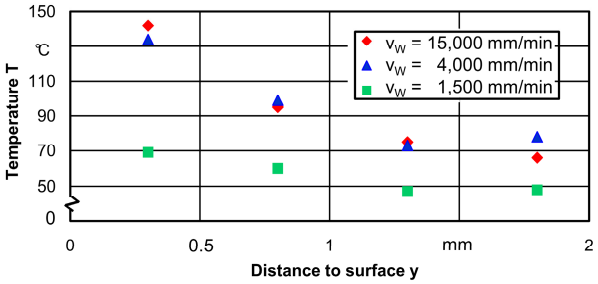

Cutting speed:	v_c = 50 m/s	Grinding wheel:	1F1 B126 VSS V360
Width of cut:	a_p = 0.1 mm	Coolant lubricant:	Non-water-based coolant
Depth of cut:	a_e = 1 mm	Process kinematics:	Down grinding
Material:	X210Cr12	Workpiece velocity:	v_W

Fig. 6.5 Dependency of temperature on the distance between the thermocouple and the contact area [8]

is constantly changing. Temperature development at the contact area of these convex surfaces is similar to the development of the process force along the grinding path. The temperature increases with an enlargement of the contact area (Fig. 6.6) [8].

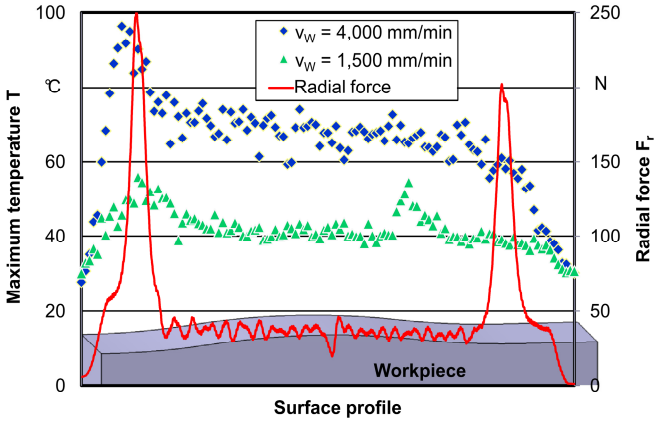

Cutting speed:	v_c = 50 m/s	Grinding wheel:	1F1 B126 VSS V360
Width of cut:	a_p = 0.1 mm	Coolant lubricant:	Non-water-based coolant
Depth of cut:	a_e = 1 mm	Process kinematics:	Down grinding
Material:	X210Cr12	Workpiece velocity:	v_W

Fig. 6.6 Temperature development over workpiece length during shape grinding

6.3 Modeling and Simulation

For modeling the numerically controlled (NC) shape grinding process a holistic approach is chosen. Consequently the reciprocal effects between structure and process are considered. In line with the present state of research, simulation of the

process is conducted by linking two simulation tools. The geometric-kinematical simulation describes the contact area A_{wgk} between the grinding wheel and the workpiece under idealized conditions. A finite element simulation takes the dynamics of the process into account.

The complete simulation consists of three parts: the geometric-kinematical simulation, the finite element simulation and the removal predictor. The interaction of these three parts is illustrated in Fig. 6.7 and described in this section. The geometry, the material properties and the NC-data are the main inputs of the simulation. The surface of the workpiece after the grinding process is the main output. It is mainly determined by the actual depth of cut $a_{e,act}$. The displacement of the grinding wheel and the process forces are additional results.

The global simulation is controlled by the geometric-kinematical simulation. Consequently, the global temporal discretization is implemented here. At the moment, equal time steps are used for the geometric-kinematical simulation and for the finite element simulation. Later on, it may become necessary to use smaller time steps for the finite element simulation in order to increase the accuracy.

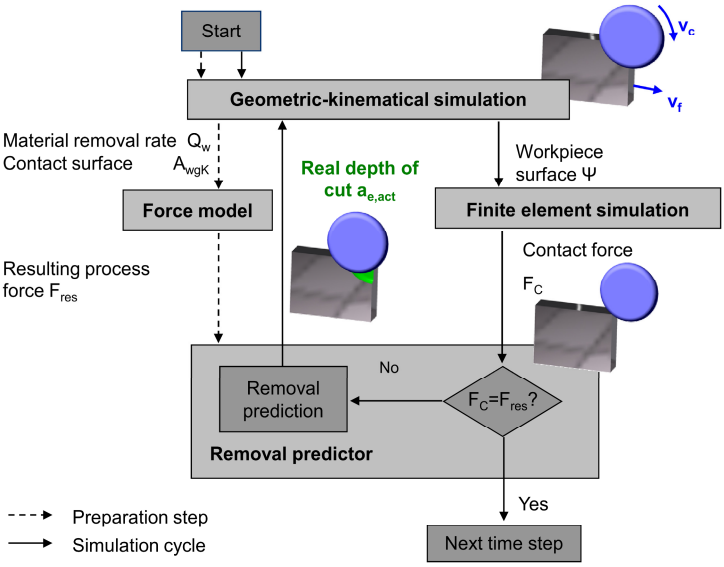

Fig. 6.7 The simulation cycle in a time step

After the initialization of the different simulations, consisting mainly of the reading of the geometric data and the usual finite element preparations, time stepping starts. The simulation cycle displayed in Fig. 6.7 is passed through in each time step. It starts with the geometric-kinematical simulation. First, some preparation steps are necessary. The new position of the workpiece in relation to

the grinding wheel is determined by the NC-data. The resulting process force F_{res} in the current time step is calculated from the geometric-kinematical data. To calculate this force an empirical grinding force model is used, which is only able to predict a resulting process force. No local or microscopic effects are taken into account.

The data for the part of the workpiece surface which might be in contact with the grinding wheel is passed on from the geometric-kinematical simulation to the finite element simulation. This information is used to describe the contact constraints of the dynamic Signorini problem in the current time step. Then, the discrete problem is solved and the normal contact stress at that time is determined. The resulting accumulated contact force F_{con} is calculated from the normal contact stress and this value is returned to the removal predictor. The most important parts of the grinding machine, the grinding wheel and the spindle, are taken into account in the finite element simulation. The stiffness of the other parts of the machine is modeled by elastic bearings.

The finite element simulation is able to calculate the accumulated contact force F_{con}. Thereby, the contact area is represented in detail. F_{con} depends directly on the actual depth of cut $a_{e,act}$. So it is expected that a good approximation of $a_{e,act}$ has been found, if F_{con} and F_{res} agree. The predicted global process force F_{res} is stored in the removal predictor.

Two steps are performed in the removal predictor. First, it tests whether the accumulated contact force F_{con} and the predicted process force F_{res} match. If that is the case, the cycle is left and the next time step is started. Otherwise, a corrected value for the actual depth of cut $a_{e,act}$ is predicted and passed on to the geometric-kinematical simulation. Here, the surface of the workpiece is modified accordingly, and the cycle restarts. See [9] for more details.

6.3.1 Geometric-Kinematical Simulation

To simulate the grinding processes, various models presently exist, as described in [5]. A geometric-kinematical simulation has been developed for NC-shape grinding. The geometric-kinematical simulation aims to determine the contact situation and is based on a dexel model, which represents the varying shape of the workpiece, while the grinding wheel is represented as a solid torus. A dexel model has been described in [10]. The material removal and the contact area of the grinding wheel and the workpiece are evaluated by the instantaneous intersection of these models. Therefore, the NC-data of the tool path generated by a CAD/CAM-program can be used as input for the simulation [9, 11-13]. Fig. 6.8 shows model elements of the geometric-kinematical simulation.

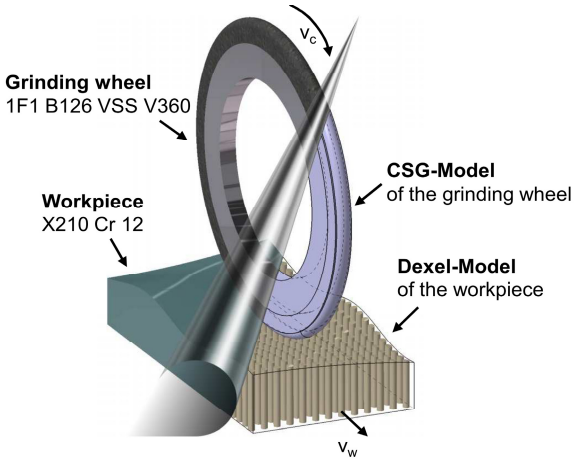

Fig. 6.8 Model elements of the geometric-kinematical simulation [2]

Force model

An empirical process force model was implemented in the geometric-kinematical simulation based on a series of experiments. A specific force model for the NC-shape grinding process based on the contact area of the geometric-kinematical simulation was developed. This empirical force model is examined under ideal conditions with deformation, vibration and temperature not being taken into account [3].

The process forces increase with an accumulating workpiece velocity in an exponential way. This behavior is analogous to the behavior of the cutting forces with defined cutting edges. Therefore, it is possible to determine a force model for the grinding process, which is based on the Kienzle equation [14], usually employed for other cutting processes.

The process forces of the NC-shape grinding are calculated fairly exactly for the geometric-kinematical simulation by the process force model. On average, the results differ by 6 % from those of the measurements. Greater deviations only appear for large contact areas. By implementing the process force model into the geometric-kinematical simulation the process forces, the contact area and the workpiece shape can be calculated and used as the basis for the finite element simulation [3].

6.3.2 Finite Element Simulation

The most relevant parts of the machine, the grinding wheel and the spindle, form the domain of the finite element model. Since their deformation is small during the grinding process a linear elastic material law is used. In addition, contact constraints have to be included in the model because the displacements of the grinding wheel are restricted by the workpiece. The dynamic behavior of the machine has to be taken into account, too. The friction between grinding wheel and

workpiece is described by Coulomb's law. Therefore, an appropriate model is given by a dynamic Signorini problem.

Besides the dynamics, thermal effects are also considered. Thus, a thermo-mechanical contact problem has to be solved, where the heat distribution and the displacement are unknown and coupled. The heat distribution is described by the heat equation. On the one hand, the displacement and the heat are interrelated by the thermo-elastic material law. On the other hand, heat is generated by the frictional contact between workpiece and grinding wheel. Mixed boundary conditions are used to model the heat transfer to the coolant. The mathematical formulation of this problem can be found in [15, 16].

The discretization of the dynamic Signorini problem can be carried out either by finite difference schemes such as the Newmark method in time and finite elements in space [16] or by finite elements in space and time [17, 18]. Both methods are implemented in the finite element library SOFAR [19], which is the platform used for the calculations described here. The discretization of the heat equation is described in [15, 16].

Precise knowledge of the workpiece surface is essential for the simulation. The workpiece surface is discretized by the nailblock model of the geometric-kinematical simulation. The finite element simulation has to evaluate this description of the surface at many different points. The nails lying in the possible contact area are taken into account in the finite element simulation. Since the coordinates of the nodes of the finite element mesh and of the nails are not identical, the evaluation has to be carried out via interpolation. Furthermore, a finite element mesh of the workpiece has to be constructed in every time step in order to calculate the heat, see [15].

Two approaches seem to be appropriate for calculating the normal and tangential contact stress. The first one is to calculate the normal and tangential contact stress based on the displacement u in a post-processing step. The second possibility is to rewrite the variational inequality as a mixed problem. Here, the normal and tangential contact stress is only the Lagrangian multiplier in the mixed problem. Thus, it is calculated in combination with the displacements during the solution process. The second formulation is preferred because a better accuracy is achieved. The tangential contact stress is the value essential for calculating the heat generated, which is proportional to the product of tangential stress and tangential velocity.

In Fig. 6.9, the finite element model and a drawing of the spindle and the grinding wheel are displayed. In the finite element model, the geometry has been slightly simplified and is discretized by hexahedral elements. The material is linear elastic in the whole domain. However, the material parameters vary. The areas where the different material parameters apply are indicated in the finite element model found in Fig. 6.9. The first region consists of the spindle and the carrier of the grinding wheel. The second one contains the grinding layer. The third region relates to the bearings. The material parameters of the bearings are used to model the stiffness of the rest of the grinding machine. This approach is explained in [20].

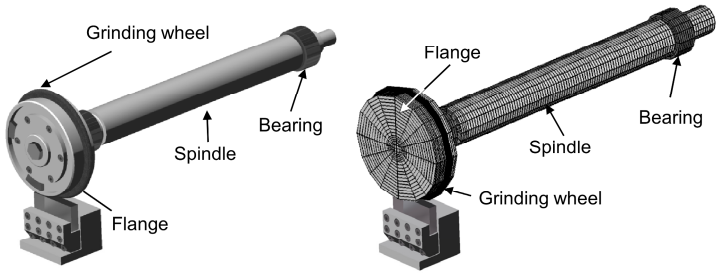

Fig. 6.9 Drawing and finite element model of the spindle and the grinding wheel

The algorithm for solving the discrete problems is complex. An extensive presentation of this theme can be found in [16]. It includes an outer fix-point algorithm, where a quadratic program with nonlinear constraints has to be solved in each iteration. Therefore, a sequential quadratic programming (SQP) method is applied. The rotation of the grinding wheel complicates the calculation. An arbitrary Lagrangian Eulerian (ALE) approach is used to take the rotational effects into account. This is also described in [16].

To discretize the thermo-elastic problem of the workpiece two points have to be considered. The first one is that the basic domain changes during the calculation due to the material removal. Consequently, the initial data of a new time step must be interpolated on the new mesh. The second point is directly related to this. A new finite element mesh has to be constructed in each time step. This is carried out by meshing the dexel model of the workpiece stored in the geometric-kinematical simulation.

The finite element simulation is complex and therefore time consuming. A posteriori error estimates have been derived and adaptive finite element methods have been developed to achieve a given accuracy at minimal numerical costs. Two different approaches are considered: In the first one, the error is estimated in the global energy norm [21-23]. This approach is easy to implement and leads to good meshes but the error is not measured in the relevant physical quantities. This disadvantage has been overcome by dual-weighted residual (DWR) based error estimators, see [18, 24]. More details can be found in Section 3.4.

6.3.3 Coupling

The target depth of cut $a_{e,tar}$ is given by the NC-data. The machine, however, is not able to realize this depth of cut. Instead, an actual depth of cut $a_{e,act}$ is measured, which is smaller than the target depth of cut. The geometric-kinematical simulation is only able to simulate the target depth of cut. It is combined with the finite element simulation to obtain a better approximation of $a_{e,act}$.

The process force F_{res} is predicted by the geometric-kinematical simulation and the contact force F_{con} is calculated by the finite element simulation. A good approximation of the actual depth of cut is found, if the contact force and the predicted process force are equal. The problem is to find such an approximation of the actual depth of cut. The solution algorithm is described in this section.

The accumulated contact force F_{con} is calculated from the actual normal contact stress by integration. The contact force F_{con} is a function of the actual depth of cut. We minimize the deviation between F_{res} and F_{con} measured in the 2-norm squared as dependent on the actual depth of cut by using the golden cut algorithm. The optimal point is then the actual depth of cut sought. For an alternative approach and more details, see [9].

6.3.4 Parametrization

Many of the model parameters, the frictional resistance coefficient and the heat distribution factors, for instance, cannot directly be determined by experiments. However, they must be accurately defined to ensure precise simulation results. Numerical parameter identification techniques are used to calculate the model parameters and to overcome the difficulties related to direct measurement.

Based on an experimental design, several suitably chosen experiments are carried out. Some quantities, which can be determined with small measurement error and calculated by the simulation, are measured. The experiments are reproduced numerically in the simulation, where some initial guesses, e. g. from literature, are used for the parameters. The difference between the simulation results and the measured results is calculated in an appropriate norm. Then, optimization algorithms are applied to minimize the deviation, where the parameters are the optimization variables. The optimal solution then gives the parameters sought.

This technique has been used to determine the damping parameters and the stiffness of the bearings. The experiments are described in [2] and the parameter identification in [20]. For the determination of the parameters connected to the model of the thermal effects, see [8, 15].

6.4 Simulation Results

During the past few years, a complex simulation has been created. It has been tested and validated step by step, i. e. every part was independently considered. Three major results are discussed here. The first one is the validation of the removal model. To this end, an actually ground workpiece surface was compared with the surface predicted by the simulation. The results of the frictional model are substantiated by the comparison of the measured tangential forces during an actual grinding process and the accumulated tangential stresses in the simulation. The third aspect relates to the simulation of thermal effects. The temperatures calculated for some chosen points of the workpiece were checked against the temperatures measured by thermocouples at the same points.

6.4.1 Validation of the Removal

The simulation presented here is tested by means of a simple grinding process. The cutting speed was set at $v_w = 50$ m/s and the workpiece velocity was $v_f = 30$ m/min. Thus, the grinding wheel rotated with $n = 85$ s^{-1}. The target depth

of cut was set at $a_e = 40$ µm. A non-water-based coolant was used. The process kinematics was down-grinding.

The simulation was carried out as described above. The termination tolerance was set at $tol = 10$ N. This seems to lead to a rough approximation. Experience with the simulation, however, has shown that a smaller tolerance changes the values of the actual depth of cut by only about $a_{e,act} = 0.001$ µm. Thus, the tolerance is accurate enough in relation to the other model errors. Three to four passes of the simulation cycle are needed to reach the given prescribed tolerance.

In Fig. 6.10, a cut through the workpiece is displayed. The measured result is also provided for comparison. Temperature effects are neglected in this calculation. One can easily see that the results are good for the quasi-stationary process phase. However, to get an accurate result during the run-in damping has to be considered in the simulation. For more details, see [2].

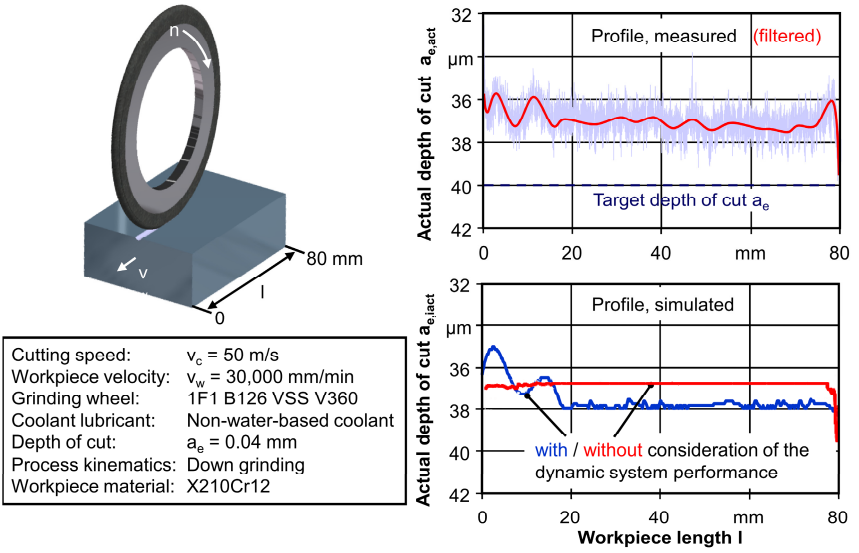

Fig. 6.10 The simulated and the actual workpiece surface

6.4.2 *Validation of the Frictional Model*

To validate the frictional model the accumulated tangential forces are calculated in the simulation and compared to the tangential forces actually measured. In Fig. 6.11, the measured forces and the simulated forces with a constant frictional coefficient and a time-dependent one are shown. In the quasi-stationary area, both approaches lead to good results. However, during the run-in and the run-out the results using the time-dependent frictional coefficient are more accurate.

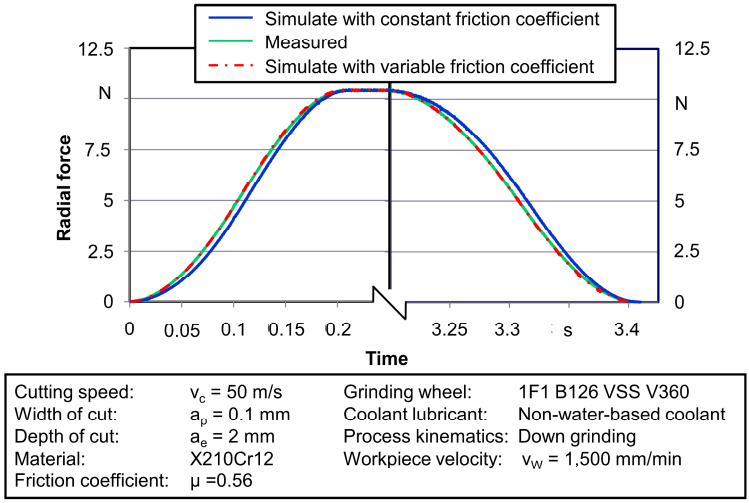

Fig. 6.11 Comparison of the tangential forces using the force model and the FEM based on the frictional model

6.4.3 Validation of the Temperature Results

In this section, the temperatures measured in an experiment are compared with the results of the corresponding simulation. A workpiece made of X210Cr12 is used. The width is 19.7 mm, the length 80 mm and the height 22.3 mm. The depth of cut is a_e of 1 mm. The material removal is carried out line-by-line, where the width of cut a_p is 0.1 mm. The cutting speed v_c is set at 50 m/s and the workpiece velocity v_w at 1,500 mm/min. The temperature of the coolant is 26°C and therefore θ_s = 26 °C is used in the simulation.

In Fig. 6.12, the temperature measured by a thermocouple is compared to the temperature calculated by the simulation at the same point. There, several passes of the grinding wheel are examined. It is obvious that the time interval between the different temperature peaks has been correctly calculated by the simulation. Furthermore, the deviation of the calculated temperature from the measured one is small. However, sometimes the simulated maximum temperature is larger than the measured one and sometimes it is smaller. The overall development was predicted correctly.

Only one pass is depicted in Fig. 6.13. There, we see that the qualitative trend of the curve for the temperatures measured is reproduced by the one simulated. The temperature decay was not predicted accurately, the temperature decay is too slow in the simulation. However, the final, resulting temperature is correct.

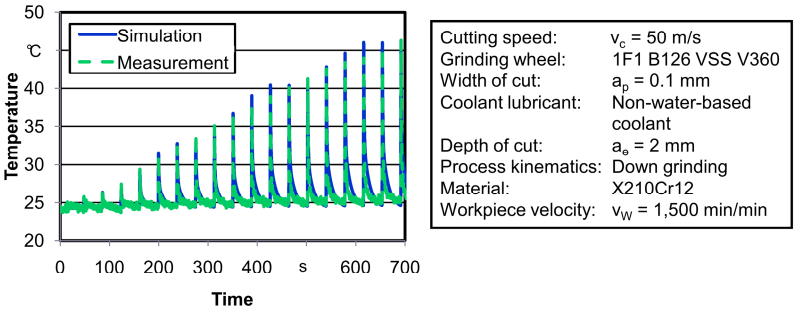

Fig. 6.12 Comparison of measured and simulated temperature results

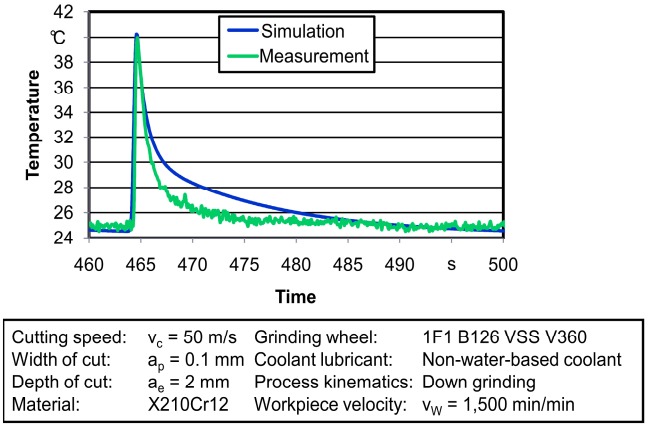

Fig. 6.13 Comparison of measurement and simulation results for one pass

6.5 Application of Simulation

In order to achieve an overall view of the simulation and the prediction of the NC data it is necessary, on the one hand, to transfer the simulation to other grinding processes and materials and, on the other hand, to integrate tool path planning into the simulation. In the following sections, the present state of path planning and the first experimental results using other grinding wheel contours will be discussed

6.5.1 Path Planning

The simulation described here was developed in order to produce, in future, an intact workpiece surface and a workpiece with a high degree of dimensional accuracy. For this purpose, path planning is integrated into the simulation. In the first step, the mean spindle displacement, when flute grinding, is examined. When producing the flutes, the depth of cut, which does not change over the grinding path, is adjusted as long as it takes for the mean actual depth of cut to reach the target

depth of cut along the grinding path. It can be seen that the simulation with path planning over a grinding path having constant engagement conditions attains the mean target cut of depth (Fig. 6.14). The positioning of the workpiece in the machine has to be examined and the traverse velocities of the different axes taken into account when path planning in order to integrate the path planning into the simulation for the changing engagement conditions and to realize the path planning for every time step.

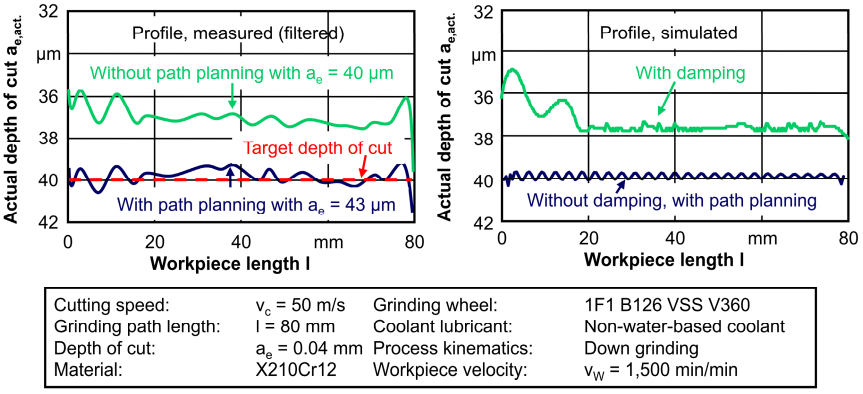

Cutting speed:	v_c = 50 m/s	Grinding wheel:	1F1 B126 VSS V360
Grinding path length:	l = 80 mm	Coolant lubricant:	Non-water-based coolant
Depth of cut:	a_e = 0.04 mm	Process kinematics:	Down grinding
Material:	X210Cr12	Workpiece velocity:	v_W = 1,500 min/min

Fig. 6.14 Flute grinding with and without path planning

6.5.2 *Transferability to Other Processes*

The simulation must be transferable to other grinding wheels and materials so that a holistic simulation can be produced. First, the different grinding processes are realized on the basis of different grinding wheel contours. In addition to a toroid grinding wheel, a cylindrical and a profile grinding wheel are used. These grinding wheels must be integrated into the simulation and analyzed to see whether the simulation is suitable. In order to calibrate the simulation force measurement must be undertaken once more to produce a force model and temperature measurements have to be made for the different grinding wheels. The different engagement conditions for the grinding wheels in the geometric-kinematical simulation are shown in Fig. 6.15.

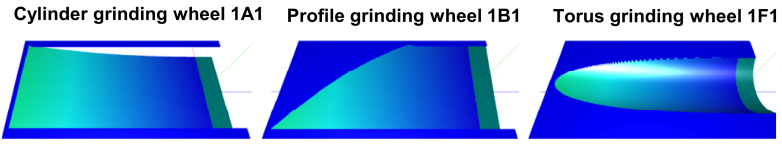

Fig. 6.15 Engagement conditions using different grinding wheels in the geometric-kinematical simulation

The forces for different process parameters are measured. Based on the mean value of the forces measured, the force coefficients at every workpiece speed for all grinding wheel contours could be determined. The simulated forces are in good agreement with the measured forces when flat surfaces are produced using cylindrical grinding wheels as well as when slanted surfaces are produced using a profile grinding wheel. Comparing the forces, it becomes obvious that there is a great variance in the forces in the area of the quickly-changing contact surfaces when concave surfaces are produced. Here, only small depths of cut can be achieved using cylindrical and profile grinding wheels (Fig. 6.16). Therefore, it is impossible to predict the forces in the simulation. The development of forces along the surface contours can be simulated using toroid grinding wheels because, due to the relatively large depth of cut, the contact surfaces are not so greatly changed as they would be for the depths of cut used with cylindrical and profile grinding wheels.

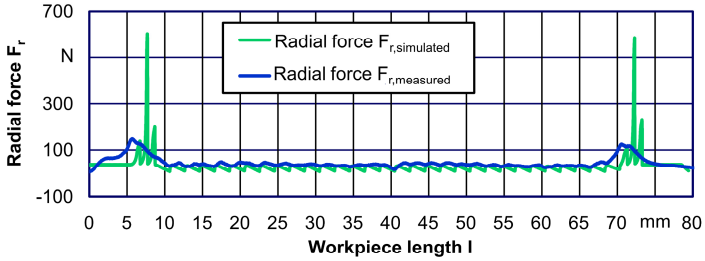

Material:	X210Cr12 (ca. 64 HRC)	Coolant lubricant:	Non-water-based coolant
Grinding wheel:	1A1 B126 VSS V360	Cutting speed:	v_c = 50 m/s
Depth of cut:	a_e = 10 µm	Workpiece velocity:	v_w = 1,500 mm/min
Width of cut:	a_p = 3 mm	Calculation accuracy:	0.0001 mm
Sampling rate:	f = 1000 Hz	Resolution of Nails:	20x20

Fig. 6.16 Comparison of the measured and simulated forces along a grinding path using a cylindrical grinding wheel for a concave workpiece

One can see that when the temperature in the process is measured the temperatures behave as described in literature and in Sect. 6.2.3 when using both grinding wheel contours. An example is shown in Fig. 6.17.

A further analysis of the grinding processes is now in progress. On the one hand, the temperatures measured using the different grinding wheel contours are being compared with the temperatures calculated in the finite element simulation. On the other hand, other workpieces are being investigated.

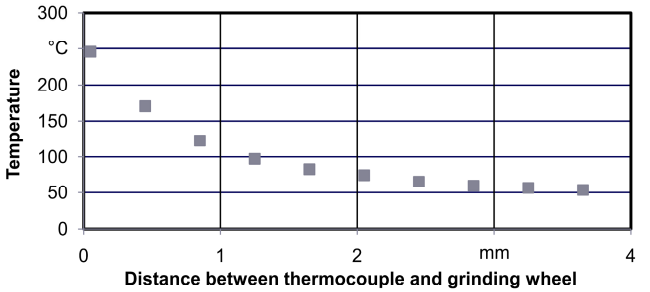

Cutting speed:	v_c = 50 m/s	Grinding wheel:	1B1 B126 VSS V360
Width of cut:	a_p = 0.1 mm	Coolant lubricant:	Non-water-based coolant
Depth of cut:	a_e = 3 mm	Process kinematics:	Down grinding
Material:	X210Cr12	Workpiece velocity:	v_W = 1,500mm/min
Profile angle:	p_w = 10°		

Fig. 6.17 Dependency of temperature on the distance between the thermocouple and the contact area using a profile grinding wheel

6.6 Conclusion and Outlook

In this chapter, the experimental basis of the empirical models for NC-shape grinding process are presented, the models themselves and also the numerical methods for calculating approximate solutions have been described. The results of three validation experiments presented here have shown that our method for simulating the NC shape grinding process is an appropriate one. In particular, the identification of model parameters using numerical methods leads to the achievement of acceptable results. Furthermore, first results concerning path planning show that the simulation approach is applicable for optimizing the process. The demonstrated transferability of the simulation approach to other grinding processes reveals the flexibility of this approach.

The application of the simulation presented here for optimizing grinding processes will be extended. As an example, complex automatic modifications of the NC data should be mentioned. One aim is to damp out oscillations in the machine structure but the restrictions of the grinding machine, which influence a realization of the NC data turn this into a difficult task. For this purpose, a lot of simulation runs are needed, where the accuracy requirements vary strongly from a rough approximation of the removal to a precise prediction of the temperature distribution. Consequently, a wide range of simulation options has to be provided and the computing time minimized. It is planned to employ adaptive finite element methods and modern high performance computing techniques to meet these demands.

Considering the practical usage of this simulation outside academic research, the key issue is the transferability of the approach to other grinding machines, other workpieces and other grinding processes. The results presented here concerning this topic will be extended by conducting further experiments, which will mainly concentrate on new workpiece materials.

References

[1] DIN EN 8589-11. Schleifen mit rotierendem Werkzeug - Einordnung, Unterteilung, Begriffe. Beuth Verlag (2003)
[2] Jansen, T.: Entwicklung einer Simulation für den NC-Formschleifprozess mit Torusschleifscheiben. Dissertation, Technische Universität Dortmund. Vulkan Verlag, Essen (2007)
[3] Biermann, D., Blum, H., Jansen, T., Rademacher, A., Scheidler, A., Weinert, K.: Experimental analyses to develop models for NC-shape grinding with a toroid grinding wheel. In: Denkena, B. (ed.) The 1st International Conference on Process Machine Interactions, Hannover, Germany, pp. 279–287, 3.9–4.9 (2008)
[4] Brecher, C., Esser, M., Witt, S.: Interaction of manufacturing process and machine tool. CIRP Annals 58(2), 588–607 (2009)
[5] Brinksmeier, E., Aurich, J.C., Govekar, E., Heinzel, C., Hoffmeister, H.-W., Peters, J., Rentsch, R., Stephenson, D.J., Uhlmann, E., Weinert, K., Wittmann, M.: Advances in modelling and simulation of grinding processes. CIRP Annals 55(2), 667–696 (2006)
[6] Klocke, F.: Manufacturing Processes 2: Grinding, Honing, Lapping. Springer, Berlin (2009)
[7] Tönshoff, H.K., Peters, J., Inasaki, I., Paul, T.: Modelling and simulation of grinding processes. CIRP Annals 41(2), 677–688 (1992)
[8] Biermann, D., Blum, H., Rademacher, A., Scheidler, A.V.: Simulation of thermal effects in NC-shape grinding of free formed surfaces using toroid grinding wheels. Part I: Experimental results. In: Proceedings of the CIRP 2nd International Conference Process Machine Interactions, Vancouver, BC, Canada, pp. 10.6–11.6 (2010); digital published
[9] Weinert, K., Blum, H., Jansen, T., Rademacher, A.: Simulation based optimization of the NC-shape grinding prozess with toroid grinding wheels. Production Engineering – Research and Development 1(3), 245–252 (2007)
[10] Stautner, M.: Simulation und Optimierung der mehrachsigen Fräsbearbeitung. Technische Universität Dortmund. Vulkan Verlag, Essen (2006)
[11] Aurich, J.C., Biermann, D., Blum, H., Brecher, C., Carstensen, C., Denkena, B., Klocke, F., Kröger, M., Steinmann, P., Weinert, K.: Modelling and simulation of process machine interaction in grinding. Production Engineering – Research and Development 3(1), 111–120 (2009)
[12] Biermann, D., Mohn, T.: A geometric-kinematical approach for the simulation of complex grinding processes. In: CIRP International Conference on Intelligent Computation in Manufacturing Engineering, Innovation and Cognitive Production Technology and Systems, Naples, Italy (2008)
[13] Weinert, K., Blum, H., Jansen, T., Mohn, T., Rademacher, A.: Angepasste Simulationstechnik zur Analyse NC-gesteuerter Formschleifprozesse. ZWF, Zeitschrift für wirtschaftlichen Fabrikbetrieb 101(7/8), 422–425 (2006)
[14] Kienzle, O.: Einfluss der Wärmebehandlung von Stählen auf die Hauptschnittkraft beim Drehen. Stahl und Eisen 74, 530–551 (1954)
[15] Biermann, D., Blum, H., Rademacher, A., Scheidler, A.V.: Simulation of thermal effects in NC-shape grinding of free formed surfaces using toroid grinding wheels. Part II: Modeling and FE-discretization. In: Proceedings of the CIRP 2nd International Conference Process Machine Interactions, Vancouver, BC, Canada, pp. 10.6–11.6 (2010); digital published

[16] Blum, H., Kleemann, H., Rademacher, A., Schröder, A.: On solving frictional contact problems part II: Dynamic case. Ergebnisberichte Angewandte Mathematik 377, Technische Universität Dortmund (2008)

[17] Blum, H., Jansen, T., Rademacher, A., Weinert, K.: Finite elements in space and time for dynamic contact problems. International Journal for Numerical Methods in Engineering 76, 1632–1644 (2008)

[18] Rademacher, A.: Adaptive Finite Element Methods for Nonlinear Hyperbolic Problems of Second Order. Dissertation Technische Universität Dortmund. Verlag Dr. Hut, München (2009)

[19] Blum, H., Kleemann, H., Rademacher, A., Schröder, A., Wiedemann, S.: SOFAR: Scientific object oriented finite element library for application and research. Technical report, Technische Universität Dortmund (2002), `http://www.mathematik.uni-dortmund.de/lsx/research/software/sofar/index.html`

[20] Biermann, D., Blum, H., Rademacher, A., Schäckelhoff, M., Scheidler, A.V., Weinert, K.: Bestimmung der Materialparameter des Spindel-Schleifscheiben-Systems mittels numerischer Parameteridentifikation. Ergebnisberichte Angewandte Mathematik 376T, Technische Universität Dortmund (2008)

[21] Biermann, D., Blum, H., Jansen, T., Rademacher, A., Scheidler, A.V., Schröder, A., Weinert, K.: Space adaptive finite element methods for dynamic Signorini problems in the simulation of the NC-shape grinding process. In: Denkena, B. (ed.) 1st International Conference on Process Machine Interactions, Hannover, Germany, pp. 309–316, 3.9.–4.9 (2008)

[22] Blum, H., Rademacher, A., Schröder, A.: Space adaptive finite element methods for dynamic Signorini problems. Electronic Transactions on Numerical Analysis 32, 162–172 (2008)

[23] Blum, H., Rademacher, A., Schröder, A.: Space adaptive finite element methods for dynamic Signorini problems. Computational Mechanics 44(4), 481–491 (2009)

[24] Rademacher, A., Schröder, A.: Goal-oriented error control in adaptive mixed FEM for Signorini's problem. Computer Methods in Applied Mechanics and Engineering 200(1-4), 345–355 (2011)